Chemical Science

Accepted Manuscript

This article can be cited before page numbers have been issued, to do this please use: M. Pal, P. Karak, D. Hati, M. Giri, S. J. George and J. Choudhury, *Chem. Sci.*, 2026, DOI: 10.1039/D6SC02610A.

ROYAL SOCIETY OF CHEMISTRY

rsc.li/chemical-science

View Article Online
DOI: 10.1039/D6SC02610A

ARTICLE

Inducing Configurational Stability in Inherently Flexible Expanded Heterohelicenes and Unlocking Stimuli-Responsive Chiroptical Switching†

Received 00th January 20xx,
Accepted 00th January 20xx

DOI: 10.1039/x0xx00000x

Manisha Pal,[a#] Pirudhan Karak,[a#] Debranjan Hati,[b] Mrityunjay Giri,[a] Subi J. George,*[b] and Joyanta Choudhury*[a]

"*π-Expanded*" (hetero)helicenes attracted special attention by virtue of their increased helical diameter, enlarged cavity, structural flexibility, and dynamics. However, their structural flexibility results in low enantiomerization barriers ($\Delta G_e^{\ddagger}$ <20 kcal·mol^{-1}), imposing a significant challenge to their enantiomeric separation, and hence the study of chiroptical properties. Therefore, there is a rising interest in increasing $\Delta G_e^{\ddagger}$ of "*π-expanded*" (hetero)helicenes, enabling their chiral separation and chiroptical study. Previously, we disclosed a new type of expanded poly-aza[9]helicenes, which possess low $\Delta G_e^{\ddagger}$ (17-18 kcal·mol^{-1}) at 25 °C, and thus the *P* and *M* enantiomers are difficult to separate, suggesting the requirement of suitable structural modification. Herein, addressing this problem, we reported the synthesis of configurationally-stable analogues of the expanded poly-aza[9]helicenes by introducing bulky *tert*-Bu groups at the terminal overlapping rings to restrict ring-flapping. The $\Delta G_e^{\ddagger}$ values for these compounds are significantly higher (>35 kcal·mol^{-1}), allowing the *P*/*M* enantiomer separation by chiral-HPLC. They show g_{abs} = 3 × 10^{-3} and g_{lum} = 5 × 10^{-3}, and stable chiroptical properties at elevated temperatures. Moreover, the basic imidazole units within these novel poly-aza[9]helicenes enabled *pH*-responsive chiroptical switching. Overall, the stable chiroptical property and stimuli-responsive chiroptical function of this class of expanded poly-aza[9]helicenes could make them promising candidates for potential chirality-based applications.

Introduction

Helicenes are among the class of "molecules in distress",[1] as they "suffer" a significant steric strain between the terminal rings of their winding structure, leading to a conformational distortion of the π-conjugated polycyclic arene framework. However, this "suffering" is complemented with chirality, one of the most intriguing properties in chemical structures, stemming from the handedness of their helical shape. It is this chirality that endows the helicenes with the fascinating chiroptical properties such as circular dichroism (CD) and circularly polarized luminescence (CPL). Varieties of emerging (opto)electronic applications are associated with the efficient CD/CPL properties, and consequently, there is an extensive research interest in developing helicene compounds suitable as materials for such applications.[2] For practical applications, configurational stability with a high racemization barrier is the basic requirement.[3] There have been several developments in the world of archetypal helicenes (possessing only angularly/*ortho*-fused rings along the helical backbone) toward isolating enantiopure compounds and studying their chiroptical properties (Fig. 1A), which have led to cutting-edge applications in materials science.[1b,1c,4] Very recently, a novel class of helicenes, called "expanded" (possessing both linearly- and angularly-fused rings along the helical rim) carbohelicenes (all-carbon helicenes)/heterohelicenes (heteroatom/s-containing helicenes) have been introduced in this field, to enrich structural diversity, modulate electronic and optoelectronic properties, dynamic chirality, and superior chiroptical properties (Fig. 1A).[5] However, the inherent flexibility in these expanded versions, owing to their enlarged helical diameter, challenged the separation/isolation of the enantioenriched compounds and the study of their chiroptical properties, because of their low $\Delta G_e^{\ddagger}$ values ($\Delta G_e^{\ddagger}$ <20 kcal·mol^{-1}) (Fig. 1A-B). Therefore, in order to obtain enantiomerically pure expanded helicenes at ambident temperature with high $\Delta G_e^{\ddagger}$ values ($\Delta G_e^{\ddagger}$ >35 kcal·mol^{-1}), commonly employed strategies are: (a) increasing the length of the helical chain, (b) π-extension at the periphery of the helicenes, (c) multiplexing helicenic motifs on the same parent helicene backbone, and (d) bulky group substitution at the internal or terminal rings of the helical backbone.[6,5e] However, the examples of enantiomerically pure expanded carbohelicenes are limited, [7]

[a]*Organometallics & Smart Materials Laboratory, Department of Chemistry, Indian Institute of Science Education and Research (IISER) Bhopal, Bhopal 462 066, India. E-mail: joyanta@iiserb.ac.in.*
[b]*New Chemistry Unit and School of Advanced Materials Jawaharlal Nehru Centre for Advanced Scientific Research (JNCASR),…… Bangalore 560064, India, E-mail: george@jncasr.ac.in*
 # M.P. and P.K. contributed equally to this work
† Electronic Supplementary Information (ESI) available: Supporting experimental procedures, computational details, and spectral details. See DOI: 10.1039/x0xx00000x

View Article Online
DOI: 10.1039/D6SC02610A

ARTICLE

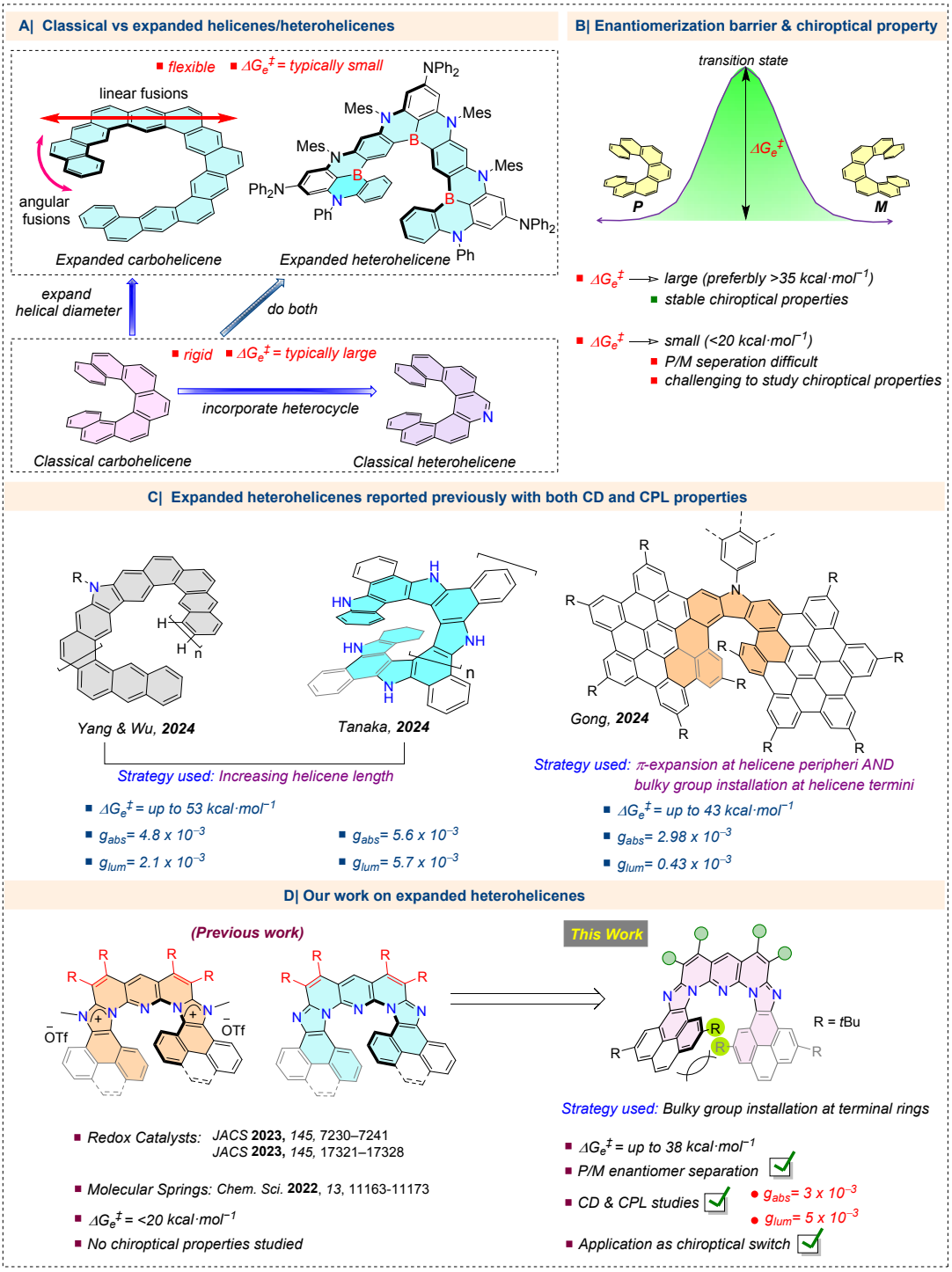

Fig. 1. (A) Examples of classical and expanded (hetero)helicenes. (B) Enantiomerization barrier and chiroptical properties of helicenes. (C) Examples of reported expanded heterohelicenes and their chiroptical properties. (D) Our earlier work and the key strategy and features of this work on expanded heterohelicenes.

View Article Online
DOI: 10.1039/D6SC02610A

ARTICLE

and expanded heterohelicenes with a high racemization barrier have been very rare until now.[5f,8,9] Just recently, in 2024, three independent studies by Yang and Wu,[5f] Tanaka,[8a] and Gong,[9] reported expanded heterohelicenes with high $\Delta G_e^{\ddagger}$ values (Fig. 1C). The previously mentioned strategies have been exploited in these works to achieve the required racemization barrier value and hence excellent absorption and luminescence dissymmetry factors. Notably, all of these expanded heterohelicenes possess carbazole as the heterocycle in their helical backbone. Systems incorporating electronically diverse heterocycles are highly desired in order to explore not only modulated CD/CPL properties but also new chiroptical functions such as stimuli-responsive chiroptical switches (*vide infra*).

Recently, we developed a double 'rollover π-expansion' (RoPE) strategy-enabled synthesis of an intriguing class of neutral and cationic "expanded" poly-azahelicenes, embedded with imidazole/imidazolium-fused pyridine-based mixed heterocyclic scaffold (Fig. 1D).[10] While the cationic systems were exploited as a novel class of redox-active electrocatalysts for CO_2-reduction reaction (CO_2RR) and hydrogen evolution reaction (HER),[11] the neutral compounds were used as stimuli (*p*H and light)-controlled soft molecular springs due to their flexible helical backbone.[10b] The same flexibility of these expanded heterohelicenes prevents the configurational stability (calculated $\Delta G_e^{\ddagger}$ value <20 kcal·mol^{-1} at 25 °C). We endeavoured to achieve the configurationally stable version of our expanded heterohelicenes by introducing bulky tertiary butyl groups at the overlapping terminal rings of the helical rim (strategy (d) as mentioned above) (Fig. 1D). Consequently, we successfully demonstrated the separation and isolation of the *P* and *M* enantiomers and evaluated the chiroptical properties, and finally, to showcase an application potential, uncovered a highly reversible on/off chiroptical switching function with the enantioenriched compounds by capitalizing on the embedded *p*H-responsive imidazole moieties (Fig. 1D).

Results and discussion

Synthesis

The precursor for the target helicenes, 2,6-bis(2,7-di-tert-butyl-9H-pyreno[4,5-*d*]imidazol-9-yl)pyridine (**PYBIM**) was synthesized by the reaction of 2,6-difluoropyridine with 2,7-di-tert-butyl-9H-pyreno[4,5-*d*]imidazole under basic conditions (Schemes S1-S4, see ESI for details). The targeted expanded poly-aza[9]helicenes, **HELI-1** and **HELI-2**, were obtained in good yields (62-73%) by applying our 'rollover π-expansion' protocol with $[RhCp^*Cl_2]_2$ catalyst on the precursor **PYBIM** with two different internal alkynes (Fig. 2A). Both the compounds **HELI-1** and **HELI-2** were well characterized by NMR spectroscopy and mass spectrometry studies (See ESI for details).

Crystal structure

The helical structure of **HELI-1** (Fig. 2B) was unambiguously confirmed by single-crystal X-ray diffraction (SCXRD) analysis, using suitable crystals grown by diffusing hexane into a dichloromethane solution of the compound at room temperature. The crystal packing profile revealed alternating stacks of both the *P* and *M* enantiomers aligned along the vertical axis, resulting in a racemic columnar structure (Fig. 2C). At the molecular level, analysis revealed that the helical pitch (d_{AI}), the vertical distance between the two terminal rings of **HELI-1** was 4.64 Å, which was much higher than our previously reported non-^{t}Bu expanded heterohelicene analogue **HELI-3** (d_{AI} = 3.66 Å).[10b] The intersecting angle (θ_{AI}) between the two planes passing through the two terminal rings was 37.2°, which is markedly larger than that (17.4°) of **HELI-3**. The torsion angles of two helicinic wings were 10.9° and 13.8°, exceeding those observed for **HELI-3** (9.4° and 12.8°). These higher values of the helical pitch, angle, and torsion angles in **HELI-1** were attributed to the presence of the bulky *tert*-butyl groups on the overlapping terminal rings of the helicene rim, which imposed severe steric hindrance between these two rings. Although we could not obtain the high quality single crystals suitable for the high quality diffraction data for **HELI-2** despite several attempts, the gross structure showed similar features like that of **HELI-1** (see ESI for details). The above structural characteristics suggested the incorporation of the desired rigidity in the inherently flexible helicenic backbone of these expanded heterohelicenes **HELI-1** and **HELI-2**. Indeed, the molecular spring constant (k) value of **HELI-1**, calculated by the density functional theory (DFT) method (Fig. 2D and Fig. S5 in ESI), was found to be 2.25 N·m^{-1}, which was significantly higher than that (k = 1.64 N·m^{-1}) of **HELI-3**, supporting the ^{t}Bu groups-induced reduction of the flexibility of the helical rim in the former compound. Overall, it appeared that the presence of the bulky ^{t}Bu groups at the two terminal overlapping rings should be able to restrict the easy flapping of the terminal rings to a great extent, and therefore, a high enantiomerization barrier was anticipated. Therefore, we investigated the enantiomerization barrier for **HELI-1** by DFT using dichloromethane solvent at 298.15 K (Fig. 2E). The $\Delta G_e^{\ddagger}$ value was found to be 38.2 kcal·mol^{-1}, which was expectedly much higher compared to **HELI-3** ($\Delta G_e^{\ddagger}$ = 16.5 kcal·mol^{-1} at 25 °C), and many other reported expanded carbo/heterohelicenes, such as expanded [13]-helicene[5c] ($\Delta G_e^{\ddagger}{}_{theory}$ = 13.0 kcal·mol^{-1} at 25 °C), the aza-

View Article Online
DOI: 10.1039/D6SC02610A

bora[9]-helicene[7a] ($\Delta G_e^{\ddagger}{}_{theory}$ = 14.3 kcal·mol^{-1} at 25 °C) and [7]-heliphene[12] ($\Delta G_e^{\ddagger}{}_{experimental}$ = 12.6 kcal·mol^{-1} at −27 °C). Similarly, the DFT calculated enantiomerization barrier of **HELI-2** was found to be 39.1 kcal·mol^{-1} (Fig. S4, ESI), comparable to that of **HELI-1**.

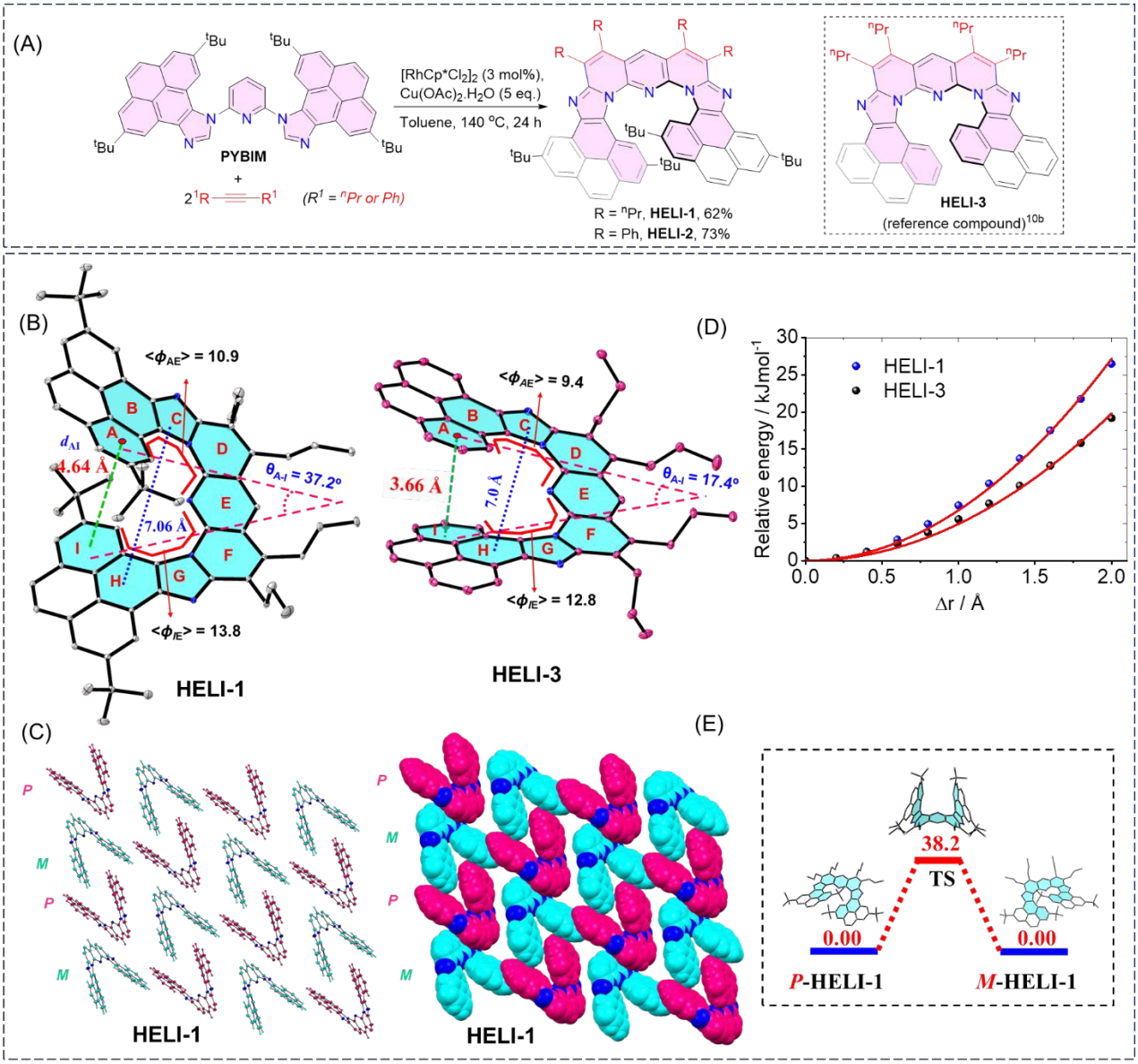

Fig. 2. (A) Synthesis of π-expanded poly-aza[9]helicenes **HELI-1** and **HELI-2**. The reference non-^{t}Bu analogue compound **HELI-3** (reported previously by our group[10b]) is shown also. (B) Crystal structures and comparison of key metric parameters of **HELI-1** (CCDC 2485128) and **HELI-3**. (C) Crystal packing and space-filling diagrams of **HELI-1**, showing the arrangement of the *P/M* isomers in the crystalline state. (D) Spring constant plots of **HELI-1** and **HELI-3**.[10b] (E) Enantiomerization energy barrier (kcal·mol^{-1}) of **HELI-1**, computed by DFT method (B3LYP/6-311g (2d,p) level of theory). TS = transition state. See ESI for details.

View Article Online
DOI: 10.1039/D6SC02610A

ARTICLE

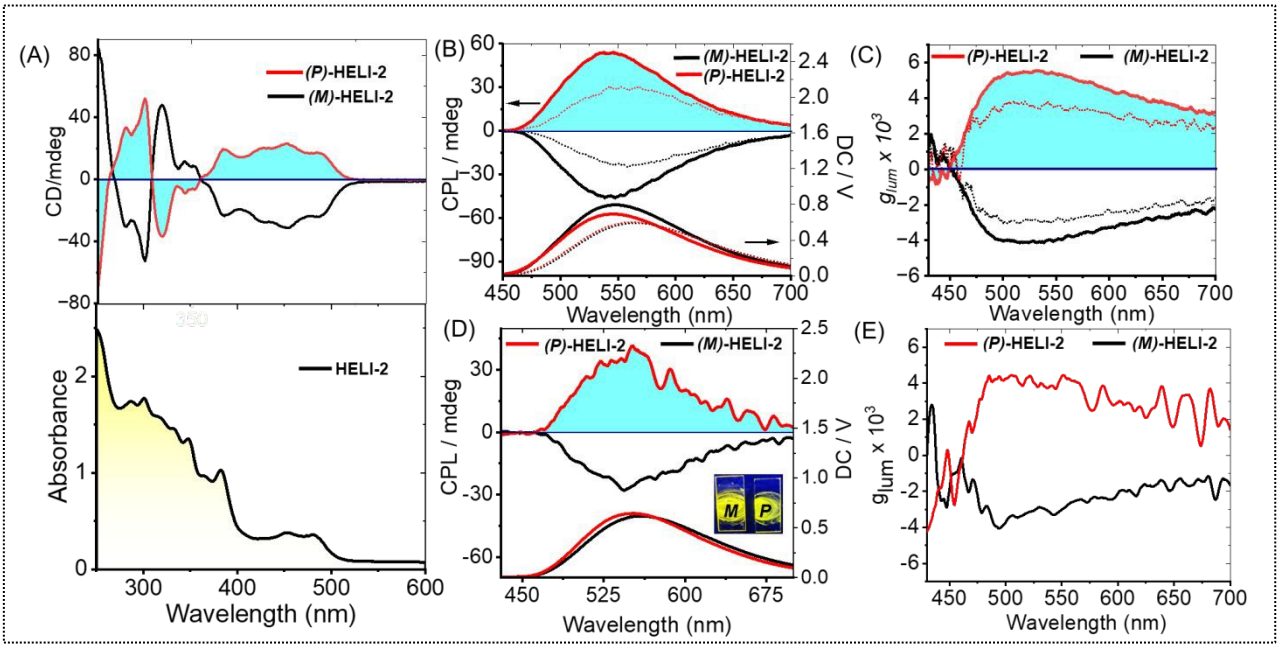

Fig. 3. (A) Absorption (bottom) of **HELI-2** and CD (top) spectra of (*P*/*M*)-**HELI-2** in hexane (18.0 μM). (B) CPL spectra (top; with left-hand-side Y-axis) and corresponding DC volt spectra (bottom; with right-hand-side Y-axis) of (*P*/*M*)-**HELI-2** in hexane (solid line) and in DCM (dotted line) (18.0 μM). (C) Luminescence dissymmetry factors of (*P*/*M*)-**HELI-2** in hexane (solid line) and in DCM (dotted line); excitation: 330 nm. (D) CPL spectra (top; with left-hand-side Y-axis) and corresponding DC volt spectra (bottom; with right-hand-side Y-axis) of (*P*/*M*)-**HELI-2** in solid thin film. (E) Luminescence dissymmetry factors of (*P*/*M*)-**HELI-2** in solid thin film.

Chiroptical properties

The sufficiently high $\Delta G_e^{\ddagger}$ value indicated the possibility of chiral resolution of the *P* and *M* enantiomers of these new expanded poly-[9]azahelicenes. At first, we chose **HELI-2** for investigating chiral resolution and follow-up chiroptical properties. After a thorough screening of conditions, the *P* and *M* enantiomers of **HELI-2** were successfully resolved by chiral HPLC using a Daicel CHIRALPAK IA-3 column and *n*-hexane/^{i}PrOH (90:10, v/v) as the eluent (Fig. S7a-c, ESI). The chiroptical properties and performances of the isolated *P*/*M* enantiomers were evaluated in both solution and solid state (thin film) using both CD and CPL studies.

The UV-vis absorption and CD spectra of the isolated enantiomers (*P*/*M*) of **HELI-2** are shown in Fig. 3A. The compound showed intense absorption bands at 350-375 nm and also at 430-500 nm (ε = 54510 M^{-1} L cm^{-1} at 355 nm; ε = 19800 M^{-1} L cm^{-1} at 445 nm in DCM; Fig. S9, ESI). The absolute configuration of *P*/*M*-**HELI-2** was determined by comparing the experimental and simulated CD spectra (calculated by using the DFT method, Fig. S65, ESI). The CD spectra of the two enantiomers expectedly showed mirror-imaged bisignated signals between 250 nm to 550 nm (*P* and *M* isomers showed positive and negative ECD, respectively, at the absorption onset). The *P*/*M*-**HELI-2** enantiomers displayed high absorption dissymmetry factors ($g_{abs} = \Delta\varepsilon/\varepsilon$) of 3×10^{-3} in hexane at 425 nm (Fig. S15, ESI), similar to many large π-extended helicenes.[5e] The linear dichroism (LD) spectra (Fig. S17 in the ESI) excluded LD contribution, which implies that there is no macroscopic alignment of the chromophore under experimental conditions in both hexane and dichloromethane. This is also supported by rotation-dependent CD spectra (Fig. S16 in ESI), where, with rotation, similar spectral features have been observed. **HELI-2** showed strong fluorescence in the 490-680 nm range with λ_{max} = 560 nm in DCM solution (Fig. S9b, ESI) and λ_{max} = 555 nm in hexane solution. The fluorescence quantum yield was calculated to be 0.38 and 0.30 in DCM and hexane, respectively (Table 4, ESI). In the DC spectra, λ_{max} = 560 nm matches with the emission spectra (Fig. 3B). The *P*/*M*-**HELI-2** showed mirror image CPL spectra λ_{max} = 550 nm in hexane, λ_{max} = 560 nm in DCM, which matches with both the emission and DC spectra (Fig. 3B). The CPL dissymetry factor g_{lum} value was measured to be 5×10^{-3} in hexane, and 3×10^{-3} in dichloromethane (Fig. 3C), which seems to be promisingly high and comparable to other relatively rigid carbo/heterohelicenes.[13, 5e, 5f, 9] As **HELI-2** was sparingly soluble in hexane, it led to molecular aggregation, which resulted in a higher g_{lum} value.[13] The dynamic light scattering (DLS) data (Fig. S18 in ESI) also suggested that the

View Article Online
DOI: 10.1039/D6SC02610A

ARTICLE

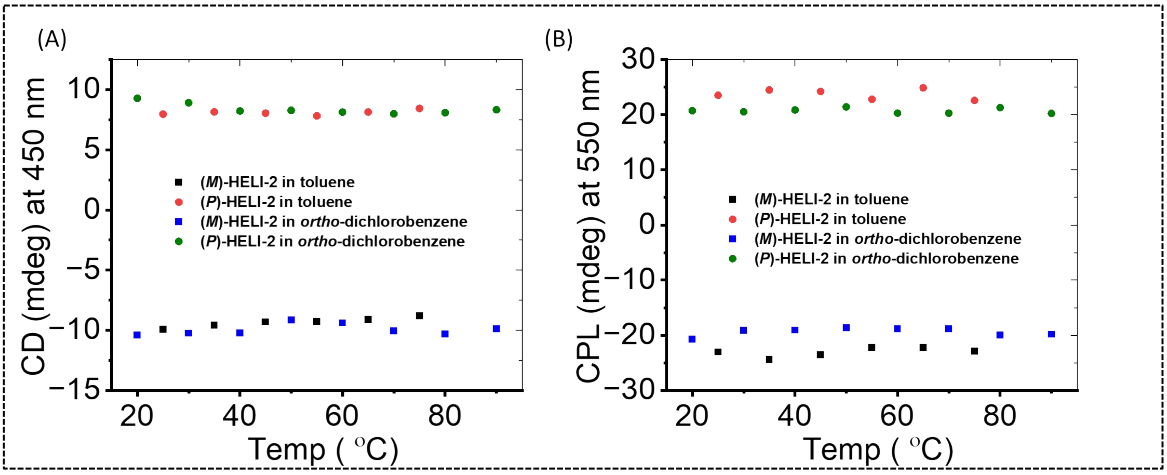

Fig. 4. (A) Change of CD signal (at 450 nm), and (B) CPL signal (at 550 nm) of (P/M)-**HELI-2** with temperature in toluene and *ortho*-dichlorobenzene solution (concentration = 8 μM).

particle size is bigger in hexane solution compared to that in DCM. Interestingly, *P* and *M* isomers of **HELI-2** showed emission in the solid-state also (Fig. 3D), and accordingly, they displayed mirror-image CPL profiles in the solid-state (drop-cast film), with a high g_{lum} value of 4 × 10^{-3} (Fig. 3E). Thus, with the encouraging chiroptical performance parameters, the *P* and *M* **HELI-2** enantiomers exhibited potential for further practical solid-state applications.

Similarly, **HELI-1** exhibited absorption bands at 320-370 nm and 420-500 nm (ε = 59900 M^{-1} L cm^{-1} at 345 nm; ε = 17600 M^{-1} L cm^{-1} at 435 nm in DCM; Fig. S8, ESI). The chiral resolution of **HELI-1** was also achieved, and the corresponding *P* and *M* enantiomers displayed mirror-image CD and CPL spectra (Fig. S12-13 ESI). For **HELI-1,** the g_{abs} and g_{lum} values are found to be 4 × 10^{-3} and 5 × 10^{-3}, respectively, in DCM (Fig. S12-14, ESI).

Temperature-dependent chiroptical properties

Stable chiroptical properties of these compounds at high temperature reinforced their suitability for further practical applications. As hexane or DCM are low-boiling solvents, toluene and *ortho*-dichlorobenzene have been used for studying temperature-dependent chiroptical properties. Before performing the experiment, we confirmed that **HELI-2** is in monomeric form in toluene by DLS study (Fig. S18 in ESI), and ensured that similar chiroptical properties have been retained, like in DCM solvent (Fig. S23 in ESI). The variation of the CD signal at 450 nm as a function of temperature was measured in toluene with a temperature gradient of 10 °C/50 min (Fig. S24-S29 in ESI). With the increase in temperature, no change in the CD signal was observed up to 75 °C (Fig. 4A), which supported the high $\Delta G_e^{\ddagger}$. In CP-OLEDs, chiral emitters often face heating issues that can affect their stability and performance during operation. Therefore, retention of CPL property at high temperatures is essential. Thus, we also measured variable temperature CPL, where no change in λ_{max} (550 nm) and CPL signal intensity was evident for both of the isomers (Fig. 4B, Fig. S38-43 in ESI) in the 25 °C–75 °C range. Also, g_{lum} value remained constant up to 75 °C (Fig. S44 in ESI). It is to note that we did not observe the decay of the CD or CPL signal in toluene solution up to 75 °C. Similarly, when *ortho*-dichlorobenzene was used as asolvent, the CD and CPL properties were retained up to 90 °C (Fig. S30-37 and S45-52 in ESI).

In addition, we have verified the stability of the representative chiral (*M*)-**HELI-2** under constant external heating at 160 °C for up to 12 h, using *ortho*-dichlorobenzene as the solvent, and monitored the CD signal at 2-hour intervals. Notably, no detectable decrement of CD signal was observed, which reconfirmed the high racemization barrier value of these expanded helicenes (Fig. S54, ESI). On that note, previously, Nowak-Król and coworkers reported azaborathia[9]helicene **H_1-Me_4**, with a racemization barrier of 39.1 kcal/mol, but no racemization was observed at 170 °C in *ortho*-dichlorobenzene as solvent.[2f]

Furthermore, the half-life ($t_{1/2}$) of the helical inversion process of **HELI-2** was evaluated at different temperatures by the DFT method (Table S2, ESI). At 25 °C, the $t_{1/2}$ value was found to be very high (~10^8 years); only at very high temperatures, such as at 300 °C, the $t_{1/2}$ value is around 5.34 minutes. This clearly indicates that the racemization of **HELI-2** can be achieved only at very high temperatures, which is experimentally very challenging.

View Article Online
DOI: 10.1039/D6SC02610A

ARTICLE

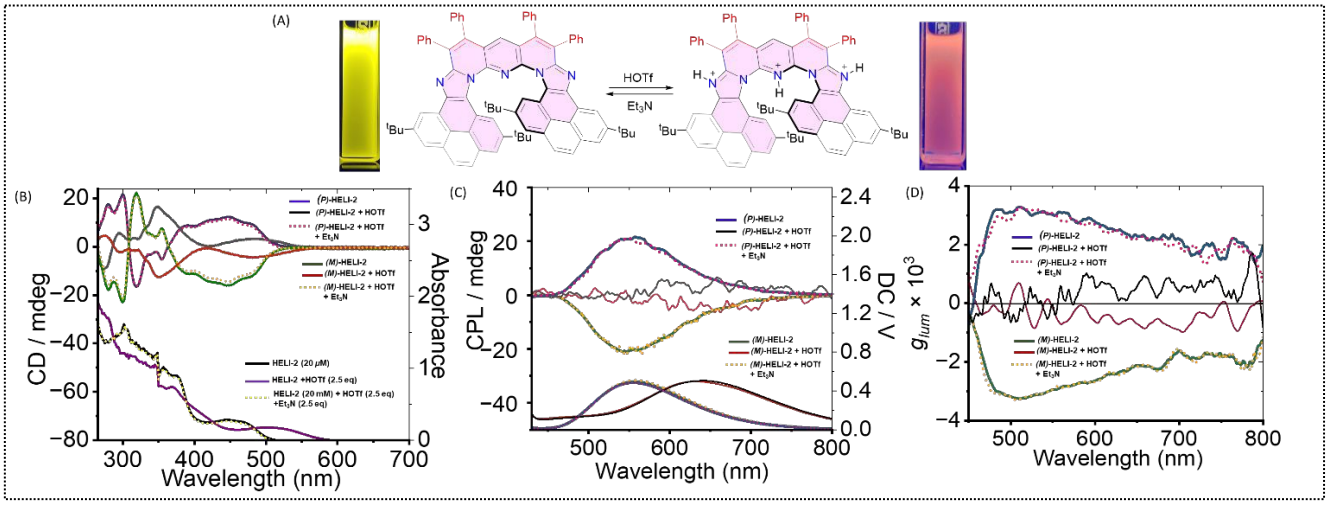

Fig. 5. (A) Acid–base responsive reversible emission property of **HELI-2** in DCM solution. (B) Absorption (bottom; with right-hand-side Y-axis) and CD (top; with left-hand-side Y-axis) spectra of (*P/M*)-**HELI-2** in DCM (8.0 μM) upon consecutive addition of acid (HOTf) and base (Et_3N). (C) CPL (top; with left-hand-side Y-axis)) and corresponding DC volt (bottom; with right-hand-side Y-axis) spectra of (*P/M*)-**HELI-2** in DCM (8.0 μM) upon consecutive addition of acid (HOTf) and base (Et_3N). (D) Luminescence dissymmetry factors of (*P/M*)-**HELI-2** in DCM (8.0 μM) upon consecutive addition of acid (HOTf) and base (Et_3N). Excitation: 330 nm.

Stimuli-responsive chiroptical switching

As mentioned earlier, this new class of expanded poly-aza[9]-helicenes, owing to the presence of the embedded *p*H-responsive imidazole moieties, opened up the opportunity to explore a stimuli (acid/base)-controlled on/off chiroptical switching function with the *P/M* enantiomers.[14] Thus, the consecutive treatment of an acid (triflic acid, CF_3SO_3H) and a base (triethylamine, Et_3N) with a solution of **HELI-2** (Fig. 5A) was first monitored by UV-Vis absorption and fluorescence spectroscopy (Fig. S55, ESI). Upon protonation, both the absorption and the emission bands of **HELI-2** red-shifted from 446 nm to 514 nm and from 560 nm to 663 nm, respectively, as the LUMO was stabilized upon protonation (Fig. 63, ESI). In the TD-DFT calculated UV-Vis spectra similar red shift was present (Fig. S64, ESI). Moreover, the protonation process was also monitored by ^{1}H NMR spectroscopic studies (Fig S60, ESI). Also, the protonated **HELI-2** showed 5 times reduced emission intensity (Fig. S55 in ESI). The original spectral profiles (both absorption and emission profiles) could be regenerated upon deprotonation by the addition of triethylamine (Fig. 5B, Fig. S55 in ESI). Next, the *p*H-responsive reversible behavior was examined with the chiral *P*/*M*-**HELI-2** isomers and monitored by CD and CPL spectroscopy. The CD spectra of *P*/*M*-**HELI-2** isomers also showed changes, with red-shifted (by 30-40 nm) peaks. Less intense bands have been observed at 350 nm and 488 nm for the protonated *P*/*M*-**HELI-2** (Fig. 5B). Upon protonation, a red shift in DC spectra has been observed (Fig. 5C). CPL signal at λ_{max} = 560 nm in DCM was found to be shifted to λ_{max} ~ 655 nm with much less CPL intensity when *P/M*-**HELI-2** isomers were treated with triflic acid (Fig. 5C). Interestingly, upon triethylamine addition, the CPL characteristics were reversibly retained (Fig. 5C), very similar to previously reported N-doped octagon-containing hexabenzocoronene (HBC) system.[14c] The acid-base responsive reversible switching behavior was also confirmed by monitoring the g_{lum} parameter of both the enantiomers (Fig. 5D), whereupon the protonation g_{lum} value was found to be reduced to ~10^{-4}. The above results demonstrated a significant stimulus-controlled chiroptical switching capability of chiroptically stable enantiomers of this new class of expanded poly-azahelicenes, which could be useful for further specialized applications in the field.

In addition, for practical applications, the main requirement is solid-state functionality.[15] So, we investigated acid-base-responsive CPL switching of **HELI-2** in the solid state (drop-cast film). Upon exposure to acid (triflic acid) vapour, the solid-state CPL intensity was found to be decreased significantly. The CPL intensity was recovered upon exposure to base (triethylamine) vapour (Fig. S62, ESI), indicating *p*H control over CPL output in solid state. These results demonstrate the viability of stimuli-responsive CPL modulation in solid-state conditions relevant to device application.

Conclusions

In conclusion, configurationally stable "π-expanded" 9-azahelicenes with a significantly enhanced enantiomerization energy barrier (>38 kcal·mol^{-1}) have been synthesized conveniently by a simple catalytic methodology. These unique helicenes can be easily separated into *P* and *M* isomers under ambient conditions. The optically pure chiral helicenes exhibited a high absorption dissymmetry factor g_{abs} (3×10^{-3} in solution) and luminescence dissymmetry factor g_{lum} (5×10^{-3} in solution and 4×10^{-3} in solid state), surpassing even those of classical [7]-helicenes. Additionally, the imidazole rings within the helicene core of these molecules enabled them with acid/base-responsive chiroptical switch properties. Crucially, the CPL properties exhibited thermal stability up to 160 °C, indicating their suitability for potential chiral applications.

Author Contributions

M. Pal: methodology, investigation, formal analysis, data curation, visualization, writing– original draft; P. Karak: methodology, investigation, formal analysis, data curation, visualization, writing–original draft; D. Hati: investigation, formal analysis, data curation; M. Giri: methodology, investigation; S. J. George: resources, supervision; J. Choudhury: conceptualization, supervision, resources, project administration, funding acquisition, writing. M. Pal, and P. Karak contributed equally to this work.

Data availability

All data of this research work are available in the manuscript and in the ESI.

Conflicts of interest

There are no conflicts to declare.

Acknowledgements

J.C. thanks the Anusandhan National Research Foundation (ANRF; erstwhile Science and Engineering Research Board, SERB), Government of India (Grant No. CRG/2022/005562), and IISER Bhopal for generous financial support. M.P. thanks Ministry of Education, Government of India for the award of the Prime Minister's Research Fellowship (PMRF). P.K. acknowledges the Integrated PhD fellowship from IISER Bhopal. D.H. thanks JNCASR for fellowship. The authors acknowledge the extensive use of NMR, Mass, and SCXRD facilities of CIF, IISER Bhopal. The authors gratefully acknowledge the High-Performance Computation (HPC) facility of IISER Bhopal for DFT calculations. The authors would also like to thank the Department of Science and Technology, Government of India for awarding the DST-FIST grant (SR/FST/CS-II/2023/312) to support NMR facilities at IISER Bhopal.

References

View Article Online
DOI: 10.1039/D6SC02610A

1 (a) R. Hoffmann and H. Hopf, *Angew. Chem. Int. Ed.*, 2008, **47**, 4474-4481; (b) M. Gingras, G. Félix and R. Peresutti, *Chem. Soc. Rev.*, 2013, **42**, 1007-1050; (c) M. Gingras, *Chem. Soc. Rev.*, 2013, **42**, 1051-1095.

2 (a) K. Dhbaibi, L. Favereau and J. Crassous, *Chem. Rev.*, 2019, **119**, 8846-8953; (b) L. Zhang, H.-X. Wang, S. Li and M. Liu, *Chem. Soc. Rev.*, 2020, **49**, 9095-9120; (c) V. Kumar, H. J. Bharathkumar, S. D. Dongre, R. Gonnade, K. Krishnamoorthy and S. S. Babu, *Angew. Chem. Int. Ed.*, 2023, **62**, e202311657; (d) S. D. Dongre, G. Venugopal, V. Kumar, A. Badrinarayan Jadhav, J. Kumar and S. Santhosh Babu, *Angew. Chem. Int. Ed.*, 2024, **n/a**, e202420767; (e) F. Zhang, V. Brancaccio, F. Saal, U. Deori, K. Radacki, H. Braunschweig, P. Rajamalli and P. Ravat, *J. Am. Chem. Soc.*, 2024, **146**, 29782-29791, (f) D. Volland, J. Niedens, P. T. Geppert, M. J. Wildervanck, F. Full, and A. Nowak-Król *Angew. Chem. Int. Ed.*, 2023, **62**, e202304291.

3 (a) P. Ravat, *Chem. Eur. J.*, 2021, **27**, 3957-3967; (b) J. M. Fernández-García, P. Izquierdo-García, M. Buendía, S. Filippone and N. Martín, *Chem. Commun.*, 2022, **58**, 2634-2645.

4 T. Mori, *Chem. Rev.*, 2021, **121**, 2373-2412.

5 (a) G. R. Kiel, S. C. Patel, P. W. Smith, D. S. Levine and T. D. Tilley, *J. Am. Chem. Soc.*, 2017, **139**, 18456-18459; (b) Y. Nakakuki, T. Hirose, H. Sotome, H. Miyasaka and K. Matsuda, *J. Am. Chem. Soc.*, 2018, **140**, 4317-4326; (c) Y. Nakakuki, T. Hirose and K. Matsuda, *J. Am. Chem. Soc.*, 2018, **140**, 15461-15469; (d) A. E. Samkian, G. R. Kiel, C. G. Jones, H. M. Bergman, J. Oktawiec, H. M. Nelson and T. D. Tilley, *Angew. Chem. Int. Ed.*, 2021, **60**, 2493-2499; (e) G. R. Kiel, H. M. Bergman, A. E. Samkian, N. J. Schuster, R. C. Handford, A. J. Rothenberger, R. Gomez-Bombarelli, C. Nuckolls and T. D. Tilley, *J. Am. Chem. Soc.*, 2022, **144**, 23421-23427; (f) G.-F. Huo, W.-T. Xu, Y. Han, J. Zhu, X. Hou, W. Fan, Y. Ni, S. Wu, H.-B. Yang and J. Wu, *Angew. Chem. Int. Ed.*, 2024, **63**, e202403149.

6 (a) P. Ravat, R. Hinkelmann, D. Steinebrunner, A. Prescimone, I. Bodoky and M. Juríček, *Org. Lett.*, 2017, **19**, 3707-3710; (b) X. Guo, Z. Yuan, Y. Zhu, Z. Li, R. Huang, Z. Xia, W. Zhang, Y. Li and J. Wang, *Angew. Chem. Int. Ed.*, 2019, **58**, 16966-16972; (c) K. Suzuki, H. Fukuda, H. Toda, Y. Imai, Y. Nojima, M. Hasegawa, E. Tsurumaki and S. Toyota, *Tetrahedron*, 2023, **132**, 133243; (d) K. Fujise, E. Tsurumaki, G. Fukuhara, N. Hara, Y. Imai and S. Toyota, *Chem Asian J.*, 2020, **15**, 2456-2461; (e) Y. Matsuo, S. Seki and T. Tanaka, *Chem. Lett.,* 2024*,* **53**, upae159.

7 (a) J. Full, S. P. Panchal, J. Götz, A.-M. Krause and A. Nowak-Król, *Angew. Chem. Int. Ed.*, 2021, **60**, 4350-4357; (b) K. Fujise, E. Tsurumaki, K. Wakamatsu and S. Toyota, *Chem. Eur. J.*, 2021, **27**, 4548-4552; (c) S. Oda, B. Kawakami, Y. Yamasaki, R. Matsumoto, M. Yoshioka, D. Fukushima, S. Nakatsuka and T. Hatakeyama, *J. Am. Chem. Soc.*, 2022, **144**, 106-112.

8 (a) Y. Matsuo, M. Gon, K. Tanaka, S. Seki, and T. Tanaka, *J. Am. Chem. Soc.*, 2024, **146**, 17428-17437; (b) J. Labella, W. R. Osterloh, K. Kuo, Y. Tsutsui, T. Tanaka and S. Seki, *J. Am. Chem. Soc.*, 2026, **148**, 9670-9679.

9 X.-Y. Wang, J. Bai, Y.-J. Shen, Z.-A. Li and H.-Y. Gong, *Angew. Chem. Int. Ed.*, 2025, **64**, e202417745.

10 (a) P. Karak, C. Dutta, T. Dutta, A. L. Koner and J. Choudhury, *Chem. Commun.*, 2019, **55**, 6791-6794; (b) P. Karak and J. Choudhury, *Chem. Sci.*, 2022, **13**, 11163-11173.

11 (a) P. Karak, S. K. Mandal and J. Choudhury, *J. Am. Chem. Soc.*, 2023, **145**, 7230-7241; (b) P. Karak, S. K. Mandal and J. Choudhury, *J. Am. Chem. Soc.*, 2023, **145**, 17321-17328.

12 S. Han, A. D. Bond, R. L. Disch, D. Holmes, J. M. Schulman, S. J. Teat, K. P. C. Vollhardt and G. D. Whitener, *Angew. Chem. Int. Ed.*, 2002, **41**, 3223-3227.

View Article Online
DOI: 10.1039/D6SC02610A

13 Z. Qiu, C.-W. Ju, L. Frédéric, Y. Hu, D. Schollmeyer, G. Pieters, K. Müllen and A. Narita, *J. Am. Chem. Soc.*, 2021, **143**, 4661-4667.
14 (a) E. Yen-Pon, F. Buttard, L. Frédéric, P. Thuéry, F. Taran, G. Pieters, P. A. Champagne and D. Audisio, *JACS Au*, 2021, **1**, 807-818; (b) Y. Matsuo, C. Maeda, Y. Tsutsui, T. Tanaka and S. Seki, *Angew. Chem. Int. Ed.*, 2023, **62**, e202314968; (c) M. A. Medel, L. Hortigüela, V. Lloveras, J. Catalán-Toledo, D. Miguel, A. J. Mota, N. Crivillers, A. G. Campaña and S. P. Morcillo, *ChemistryEurope*, 2023, **1**, e202300021.
15 (a) J. Han, S. Guo, H. Lu, S. Liu, Q. Zhao, and W. Huang, *Adv. Optical Mater.,* 2018, **6**, 1800538; (b) J. Ahn, S. H. Lee, I. Song, P. Chidchob, Y. Kwon, and J. H. Oh, *Device*, 2023, **1**, 100176.

View Article Online
DOI: 10.1039/D6SC02610A

Data Availability Statement

The data supporting this manuscript have been included as part of the Electronic Supplementary Information (ESI).

CCDC deposition number 2485128 contains the supplementary crystallographic data for this paper. These data are provided free of charge by the joint Cambridge Crystallographic Data Centre and Fachinformationszentrum Karlsruhe Access Structures service www. ccdc.cam.ac.uk/structures.